Efficient decoupling approach for reliability-based optimization based on augmented Line Sampling and combination algorithm

Xiukai Yuan[a], Marcos A. Valdebenito[b,*], Baoqiang Zhang[a,**], Matthias G.R. Faes[b], Michael Beer[c,d,e]

[a]*School of Aerospace Engineering, Xiamen University, Xiamen 361005, R.P. China*
[b]*Chair for Reliability Engineering, TU Dortmund University, Leonhard-Euler-Strasse 5, 44227 Dortmund, Germany.*
[c]*Institute for Risk and Reliability, Leibniz Universität Hannover, Callinstr. 34, Hannover, Germany*
[d]*Institute for Risk and Uncertainty, University of Liverpool, Peach Street, L69 7ZF Liverpool, United Kingdom*
[e]*International Joint Research Center for Resilient Infrastructure & International Joint Research Center for Engineering Reliability and Stochastic Mechanics, Tongji University, Shanghai 200092, China*

Abstract

This paper presents a novel decoupling approach to efficiently solve a class of reliability-based design optimization (RBDO) problems by means of augmented Line Sampling. The proposed approach can fully decouple the original RBDO by replacing the probabilistic constraint with the failure probability function (FPF), which is an explicit function of the design variables. One attractive feature is that the main numerical cost associated with this decoupling comes with only one implementation of augmented Line Sampling, which is actually highly efficient. And for the sake of accuracy, the proposed approach incorporates decoupling with the sequential optimization framework to solve the RBDO problem iteratively. On top of that, an optimal combination algorithm is proposed to reuse the information through aggregating the local estimates of FPF obtained in different iterations to produce an improved estimate, resulting in a more accurate and stable solution. Examples are given to show the effectiveness and efficiency of the proposed approach.

Keywords: Reliability-based design optimization, Augmented Line Sampling, Decoupling, Sequential optimization

1. Introduction

Reliability-based design optimization (RBDO) [1, 2] serves as an effective tool for structural design optimization under uncertainty in engineering. In essence, RBDO aims at identifying the optimal design in terms of reliability, given a set of uncertain or inherently variable model quantities. Since uncertainty and variability are rather the norm than exception in engineering cases, these methods have the potential to leverage more reliable designs. However, the widespread application of this class of methods in engineering and industrial practice is hindered by the large computational burden associated with finding the optimal design due to the need for solving a reliability problem at each step of the optimization.

Many methods have been proposed in an attempt to decrease the numerical costs associated with the solution of RBDO problems. There are mainly three kinds of methods which have been developed, namely double loop methods, single loop methods, and decoupling methods. Double loop methods [3] carry out the reliability analysis (which corresponds to the inner loop) for each step in the design optimization (i.e., the outer loop) to estimate the probability of failure of the design in the current iteration. It is clear that the computational cost of this class of methods is very high due to its nested nature. Single loop methods [4] replace the reliability analysis loop by its Karush–Kuhn–Tucker (KKT) optimality conditions. In this way, one can efficiently handle linear and moderately nonlinear performance functions. Decoupling methods replace the probabilistic constraint by constructing an explicit (and usually approximate) representation of the failure probability as a function of the design parameters. The latter is termed as the failure probability function (FPF). The key of decoupling methods is the construction of FPF, and different ways are proposed, such as making an approximation based on the sensitivity of failure probability with respect to design parameters [5], the application of pre-defined functions [6, 7], employing the idea of solving an augmented reliability problem [8, 9], and the weighted approach [10, 11]. These methods solve the reliability and optimization problem sequentially, and as such, effectively break the double loop. In addition to the three methods for solving RBDO problems described above, some of the authors very recently introduced a 'completely decoupled' method based on Operator Norm theory. This method, which is applicable for a class of linear models, is highly effective in reducing the computational cost, since it just requires the solution of a single deterministic optimisation problem followed by a single reliability analysis [12].

Concerning the reliability analysis that is employed for RBDO, many methods adopt approximate analytical approaches, e.g., reliability index approach [3, 13] and performance measure approach [14, 15]. Although analytical methods can provide an efficient estimation of the failure probability, they typically suffer from low accuracy, especially in case the governing limit-state function is highly non-linear. Simulation methods evaluate the failure probability through sampling, regardless of the nonlinearity or complexity of the structural limit state function. In this context, Monte Carlo simulation or advanced variants hereof, including, Importance Sampling [16, 17], Directional Importance Sampling [18], Subset Simulation [19] and Line Sampling [20, 21], are applied. These methods are found to be (mostly) robust with respect to the problem at hand, although a full review of their different capabilities is beyond the scope of this work. In any case, the integration of these techniques in a double-loop scheme is hindered by the corresponding computational expense. An alternative means for circumventing this issue involves surrogate methods such as, for example, response surface [22, 23] and kriging model [24, 25].

In this contribution, a new decoupling approach based on augmented Line Sampling and a optimal combination algorithm is proposed to handle the RBDO problem efficiently. Augmented Line Sampling (ALS) [26, 27] is utilized to estimate the FPF through a single Line Sampling run in an augmented space. Thus, the proposed approach adopts ALS to decouple the original RBDO by replacing the probabilistic constraint with the obtained failure probability function estimate. Then, the proposed approach incorporates decoupling with the sequential optimization framework to solve the RBDO problem iteratively. Further, a combination algorithm is proposed to integrate the local approximations obtained in previous iterations with the current one, which is expected to enhance the performance of the optimization process. The most salient features of the proposed approach are, 1) it utilizes a simulation-based reliability analysis method, which is expected to own higher accuracy than approximated methods; 2) it decouples the double loop problem, and hence is efficient; 3) only one single run of Line Sampling is required to estimate the FPF to decouple the RBDO problem, in contrast to multiple runs that would be required in a double-loop implementation; 4) a optimal combination algorithm is proposed to reuse the information in the current iteration which can further enhance the performance of the proposed approach regarding stability and convergence speed. The aforementioned features constitute a significant novelty with respect to previous contributions [26, 27]. Specifically, the work reported in [26] focuses on estimating the failure probability function, while [27] aims at solving imprecise reliability problems. However, this paper addresses the RBDO problem using the ALS method, with special focus on deocupling, information re-use and combination of reliability estimators generated at different stages.

The paper is organized as follows. The definition of the RBDO problem is presented in Section 2. Then, the mathematical formulation of the proposed decoupling approach is developed in Section 3. Then, in Section 4, various examples are presented to show the performance of the proposed approach. Finally, Section 5 lists the conclusions of the paper.

2. Reliability-based optimization problem

The RBDO problem considered in this contribution is formulated as the minimization of the cost of a structure subject to multiple probabilistic and deterministic constraints. In mathematical terms, this is cast as

$$\begin{aligned} \min \quad & W(\boldsymbol{\theta}) \\ \text{s.t.} \quad & P_{Fl}(\boldsymbol{\theta}) \le P_{Fl}^{\text{tol}} \quad && (l = 1, 2, \dots, n_P) \\ & C_j(\boldsymbol{\theta}) \le 0 && (j = 1, 2, \dots, n_C) \\ & \underline{\theta}_i \le \theta_i \le \bar{\theta}_i && (i = 1, 2, \dots, n_\theta)\,, \end{aligned} \tag{1}$$

where $W(\boldsymbol{\theta})$ is the objective function, which represents the cost W as a function of a vector of design parameters $\boldsymbol{\theta} = [\theta_1, \dots, \theta_{n_\theta}]$, corresponding to the distribution parameters (e.g., mean values) of structural random variables, the latter being denoted by $\boldsymbol{x} = [x_1, \dots, x_n]$; $C_j(\boldsymbol{\theta})$ is the j -th deterministic constraint;$P_{Fl}(\boldsymbol{\theta})$ is the probability of failure with respect to the l-th performance criterion in the $\boldsymbol{x}$ space which depends on $\boldsymbol{\theta}$ and P_{Fl}^{tol} is the corresponding l^{th} tolerance margin, also referred to as the target failure probability. The quantity $P_{Fl}(\boldsymbol{\theta})$ as a function of $\boldsymbol{\theta}$ is referred to as failure probability function (FPF). In this analysis, the random variables are assumed to be independent.

In this contribution, we focus on a particular kind of problem, where the design parameters refer to the distribution parameters of the uncertain quantities in the analysis. Such problems are encountered when, for example, the mean value of the geometrical dimensions of a given structure are taken as the design parameters in the RBDO problem. For the sake of simplicity, this paper considers a single reliability constraint, that is, $n_P = 1$. However, note that the proposed approach can handle problems with multiple reliability constraints. In such case, an approximation of FPF should be constructed for each reliability constraint. As such, $P_{Fl}(\boldsymbol{\theta})$ can be rewritten as $P_F(\boldsymbol{\theta})$, which is defined as:

$$P_F(\boldsymbol{\theta}) = \int I_F(\boldsymbol{x}) f(\boldsymbol{x} \mid \boldsymbol{\theta}) \mathrm{d}\boldsymbol{x}, \tag{2}$$

where $f(\boldsymbol{x} \mid \boldsymbol{\theta})$ is the conditioned probability density function (PDF) of $\boldsymbol{x}$ based on the parameter $\boldsymbol{\theta}$; $I_F(\boldsymbol{x})$ is the indicator function of the failure domain; $I_F(\boldsymbol{x}) = 1$ if $(\boldsymbol{x}) \in F$, and $I_F(\boldsymbol{x}) = 0$ if $(\boldsymbol{x}) \notin F$; $F = \{\boldsymbol{x} : g(\boldsymbol{x}) < 0\}$, is the failure domain, $g(\bullet)$ is the performance function.

3. Proposed approach

An efficient decoupling approach is discussed in this section to solve the RBDO problem presented in Eq. (1) without having to solve the related double-loop problem. This proposed approach features three key steps.

- The first step explained in detail in Section 3.1 is to obtain the FPF $P_F(\boldsymbol{\theta})$ based on the Augmented Line Sampling (ALS) method. In essence, it is adopted to replace the 'inner' loop of Eq. (1) by an estimated explicit relationship between $\boldsymbol{\theta}$ and $P_F(\boldsymbol{\theta})$.
- The second step is the implementation of the sequential optimization framework. This is explained in detail in Section 3.2. In essence, sequential optimization implies that the optimization problem is solved over a reduced domain of the design variables. This protects the quality of the approximation of the probability function generated with ALS. Naturally, these reduced space designs are adjusted iteratively, such that the optimization process can converge towards the sought optimal solution.
- This last step of the proposed framework consists of a newly proposed combination algorithm, as explained in detail in Section 3.3. The optimal combination algorithm is proposed to reuse the information from previous iterations of sequential optimization in the current iteration. This can further enhance the performance of the proposed approach regarding stability and convergence speed.

3.1. Augmented Line Sampling for the FPF estimation

The Augmented Line Sampling (ALS) is first presented which has been introduced by some of the authors in [26] in the context of efficiently estimating the FPF $P_F(\boldsymbol{\theta})$. As a first step in ALS, an instrumental sampling density function $f(\boldsymbol{x}|\boldsymbol{\theta}^*)$ is introduced in Eq. (2). Straighforwardly, the original PDF with a fixed nominal distribution parameter $\boldsymbol{\theta}^*$ is choosen, yielding $f(\boldsymbol{x}|\boldsymbol{\theta}^*)$. Then the formulation of the FPF $P_F(\boldsymbol{\theta})$ is rewritten as

$$P_F(\boldsymbol{\theta}) = \int I(\boldsymbol{x}) \frac{f(\boldsymbol{x}|\boldsymbol{\theta})}{f(\boldsymbol{x}|\boldsymbol{\theta}^*)} f(\boldsymbol{x}|\boldsymbol{\theta}^*) \mathrm{d}\boldsymbol{x}, \tag{3}$$

which is subsequently transformed to the standard normal space. Generally, the transformation from non-normal variables to standard normal ones (denoted by T_{xu}) and the corresponding inverse transformation (T_{ux}) are provided as:

$$\boldsymbol{u} = T_{xu}(\boldsymbol{x} \mid \boldsymbol{\theta}^*), \boldsymbol{x} = T_{ux}(\boldsymbol{u} \mid \boldsymbol{\theta}^*). \tag{4}$$

Then by inserting Eq. (4) into Eq. (3), the FPF can be rewritten as

$$P_F(\boldsymbol{\theta}) = \int I_F(T_{ux}(\boldsymbol{u} \mid \boldsymbol{\theta}^*)) \frac{f(T_{ux}(\boldsymbol{u} \mid \boldsymbol{\theta}^*) \mid \boldsymbol{\theta})}{f(T_{ux}(\boldsymbol{u} \mid \boldsymbol{\theta}^*) \mid \boldsymbol{\theta}^*)} \phi(\boldsymbol{u}) \mathrm{d}\boldsymbol{u} \tag{5}$$

$$= \int I_F(T_{ux}(\boldsymbol{u} \mid \boldsymbol{\theta}^*)) \eta(\boldsymbol{u}, \boldsymbol{\theta}, \boldsymbol{\theta}^*) \phi(\boldsymbol{u}) \mathrm{d}\boldsymbol{u}, \tag{6}$$

where $\phi(\boldsymbol{u})$ is the standard normal PDF; and

$$\eta(\boldsymbol{u}, \boldsymbol{\theta}, \boldsymbol{\theta}^*) = \frac{f(T_{ux}(\boldsymbol{u} \mid \boldsymbol{\theta}^*) \mid \boldsymbol{\theta})}{f(T_{ux}(\boldsymbol{u} \mid \boldsymbol{\theta}^*) \mid \boldsymbol{\theta}^*)}, \tag{7}$$

is the ratio of two PDFs. This integral formulation can be efficiently evaluated by means of Line Sampling. For this purpose, consider the rotated coordinate system:

$$\boldsymbol{u} = \boldsymbol{R}\boldsymbol{u}^{\perp} + \boldsymbol{\alpha} u'', \tag{8}$$

where $\boldsymbol{R}$ is a rotation matrix of dimension $n \times (n-1)$; $\boldsymbol{u}^{\perp}$ is vector of dimension $(n-1) \times 1$; $\boldsymbol{\alpha} = [\alpha_1, \alpha_2, \ldots, \alpha_n]$ is the unit important direction which is determined when the basic random variables $\boldsymbol{x}$ are distributed as $f(\boldsymbol{x}|\boldsymbol{\theta}^*)$; u'' is a scalar coordinate. Note that the criterion used in this work for selecting the important direction $\boldsymbol{\alpha}$ is discussed in detail in Section 3.2. With these considerations, the probability integral shown in Eq. (6) becomes:

$$P_F(\boldsymbol{\theta}) = \iint I_F(T_{ux}(\boldsymbol{R}\boldsymbol{u}^{\perp} + \boldsymbol{\alpha} u'' \mid \boldsymbol{\theta}^*)) \eta(\boldsymbol{R}\boldsymbol{u}^{\perp} + \boldsymbol{\alpha} u'', \boldsymbol{\theta}, \boldsymbol{\theta}^*) \phi(u'') \phi(\boldsymbol{u}^{\perp}) \mathrm{d}u'' \mathrm{d}\boldsymbol{u}^{\perp}, \tag{9}$$

where $\phi(u'')$ is standard normal PDF in one dimension; $\phi(\boldsymbol{u}^{\perp})$ is standard normal PDF in $(n-1)$ dimensions.

We can evaluate this integral by generating samples of $\boldsymbol{u}^{\perp}$ distributed according to $\phi(\boldsymbol{u}^{\perp})$, i.e., $\left\{\boldsymbol{u}^{\perp(j)} : j = 1, 2, \ldots, N\right\}$. The LS estimator $\hat{P}_F(\boldsymbol{\theta})$ of $P_F(\boldsymbol{\theta})$ can as such be computed as:

$$P_F(\boldsymbol{\theta}) \approx \hat{P}_F(\boldsymbol{\theta}) = \frac{1}{N} \sum_{j=1}^{N} \left(\int I_F(T_{ux}(\boldsymbol{R}\boldsymbol{u}^{\perp(j)} + \boldsymbol{\alpha} u'' \mid \boldsymbol{\theta}^*)) \eta(\boldsymbol{R}\boldsymbol{u}^{\perp(j)} + \boldsymbol{\alpha} u'', \boldsymbol{\theta}, \boldsymbol{\theta}^*) \phi(u'') \mathrm{d}u'' \right), \tag{10}$$

where $\int I_F(T_{ux}(\boldsymbol{R}\boldsymbol{u}^{\perp(j)} + \boldsymbol{\alpha} u'' \mid \boldsymbol{\theta}^*)) \eta(\boldsymbol{R}\boldsymbol{u}^{\perp(j)} + \boldsymbol{\alpha} u'', \boldsymbol{\theta}, \boldsymbol{\theta}^*) \phi(u'') \mathrm{d}u''$ is a one-dimension integral. Considering that

$$I_F(T_{ux}(\boldsymbol{R}\boldsymbol{u}^{\perp(j)} + \boldsymbol{\alpha} u'' \mid \boldsymbol{\theta}^*)) = \begin{cases} 1 \quad if \quad u'' \geqslant \boldsymbol{\beta}^{(j)} \\ 0 \quad if \quad u'' < \boldsymbol{\beta}^{(j)}, \end{cases} \tag{11}$$

where $\beta^{(j)}$ denotes the intersection of the line $\boldsymbol{R}\boldsymbol{u}^{\perp(j)} + \boldsymbol{\alpha} u''$ with the limit state function (which is obtained by quadratic interpolation in this contribution [20]), the aforementioned one-dimensional integral becomes:

$$\hat{P}_F(\boldsymbol{\theta}) = \frac{1}{N}\sum_{j=1}^{N}\left(\int_{\boldsymbol{\beta}^{(j)}}^{\infty} \eta(\boldsymbol{R}\boldsymbol{u}^{\perp(j)} + \boldsymbol{\alpha}u'', \boldsymbol{\theta}, \boldsymbol{\theta}^*)\phi(u'')\mathrm{d}u''\right) = \frac{1}{N}\sum_{j=1}^{N} q_1(u''), \tag{12}$$

where $q_1(u'')$

$$q_1(u'') = \int_{\boldsymbol{\beta}^{(j)}}^{\infty} \eta(\boldsymbol{R}\boldsymbol{u}^{\perp(j)} + \boldsymbol{\alpha}u'', \boldsymbol{\theta}, \boldsymbol{\theta}^*)\phi(u'')\mathrm{d}u'' \tag{13}$$

denotes the inner integral which involves one dimensional integration with respect to u''.

In this contribution, the random variables are all assumed to be independently and normally distributed, i.e., $x_i \sim N(\mu_i, \sigma_i^2)$, and the design variables are considered to be the mean values $\theta_i = \mu_i$. In this context, $x_i = T_{ux}(u_i|\theta_i^*) = u_i\sigma_i + \mu_i^* = u_i\sigma_i + \theta_i^*$, then $\eta(\boldsymbol{u}, \boldsymbol{\theta}, \boldsymbol{\theta}^*)$ in Eq. (7) becomes

$$\eta(\boldsymbol{u}, \boldsymbol{\theta}, \boldsymbol{\theta}^*) = \frac{f(T_{ux}(\boldsymbol{u}|\boldsymbol{\theta}^*) \mid \boldsymbol{\theta})}{f(T_{ux}(\boldsymbol{u}|\boldsymbol{\theta}^*) \mid \boldsymbol{\theta}^*)} = \prod_{i=1}^{n} \exp\left[\frac{(\theta_i - \theta_i^*)}{\sigma_i}u_i - \frac{(\theta_i - \theta_i^*)^2}{2\sigma_i^2}\right]. \tag{14}$$

Substitution of Eq. (8) into Eq. (14), and letting $\boldsymbol{\theta} = \boldsymbol{\mu}$ and $\boldsymbol{\theta}^* = \boldsymbol{\mu}^*$, it is possible to show that:

$$\eta(\boldsymbol{R}\boldsymbol{u}^{\perp(j)} + \boldsymbol{\alpha}u'', \boldsymbol{\mu}, \boldsymbol{\mu}^*) = \exp\sum_{i=1}^{n}\left[\frac{(\mu_i - \mu_i^*)}{\sigma_i}(\boldsymbol{R}_i\boldsymbol{u}^{\perp(j)} + \alpha_i u'') - \frac{(\mu_i - \mu_i^*)^2}{2\sigma_i^2}\right] \tag{15}$$

$$= \exp\left[\sum_{i=1}^{n}\left(\frac{(\mu_i - \mu_i^*)\boldsymbol{R}_i\boldsymbol{u}^{\perp(j)}}{\sigma_i} - \frac{(\mu_i - \mu_i^*)^2}{2\sigma_i^2}\right) + \sum_{i=1}^{n}\frac{(\mu_i - \mu_i^*)\alpha_i u''}{\sigma_i}\right] \tag{16}$$

$$= e^{\lambda^{(j)} + u''\tau^{(j)}} \tag{17}$$

where:

$$\lambda^{(j)} = \sum_{i=1}^{n}\frac{(\mu_i - \mu_i^*)\boldsymbol{R}_i\boldsymbol{u}^{\perp(j)}}{\sigma_i} - \frac{(\mu_i - \mu_i^*)^2}{2\sigma_i^2} = \sum_{i=1}^{n}\chi_i\boldsymbol{R}_i\boldsymbol{u}^{\perp(j)} - \frac{\chi_i^2}{2} \tag{18}$$

$$\tau^{(j)} = \sum_{i=1}^{n}\frac{(\mu_i - \mu_i^*)\alpha_i}{\sigma_i} = \sum_{i=1}^{n}\chi_i\alpha_i \tag{19}$$

where $\boldsymbol{R}_i$ is the i-th row of matrix $\boldsymbol{R}$; α_i is i-th component of vector $\boldsymbol{\alpha}$, and $\chi_i = \frac{\theta_i - \theta_i^*}{\sigma_i}$. Thus, we also have $u_i^{(j)} = \boldsymbol{R}_i\boldsymbol{u}^{\perp(j)} + \alpha_i u''^{(j)}$.

The integral $q_1(u'')$ in Eq. (13) can be rewritten as:

$$q_1(u'') = \int_{\boldsymbol{\beta}^{(j)}}^{\infty} e^{\lambda^{(j)}+u''\tau^{(j)}} \phi(u'')\mathrm{d}u'' \tag{20}$$

$$= e^{\boldsymbol{\lambda}^{(j)}} \int_{\beta^{(j)}}^{+\infty} e^{\tau u''} \phi(u'')\mathrm{d}u'' \tag{21}$$

$$= e^{\boldsymbol{\lambda}^{(j)}} e^{\frac{\tau^{(j)2}}{2}} \int_{\beta^{(j)}-\tau^{(j)}}^{+\infty} \phi_1(t)\mathrm{d}t \tag{22}$$

$$= e^{\boldsymbol{\lambda}^{(j)}+\frac{\tau^{(j)2}}{2}} \Phi(\tau^{(j)} - \beta^{(j)}) \tag{23}$$

Finally, this integral of the FPF can be approximated via a closed-form expression as follows:

$$\hat{P}_F(\boldsymbol{\theta}) = \frac{1}{N} \sum_{j=1}^{N} \left[e^{\lambda^{(j)}+\frac{\tau^{(j)2}}{2}} \Phi(\tau^{(j)} - \boldsymbol{\beta}^{(j)}) \right] \tag{24}$$

It can be easily derived that the estimator $\hat{P}_F(\boldsymbol{\theta})$ in Eq. (24) is unbiased. The variance and Coefficient of Variation (C.o.V.) associated with the estimator in Eq. (24) are given by

$$Var\left[\hat{P}_F(\boldsymbol{\theta})\right] \approx \frac{1}{(N-1)} \left\{ \frac{1}{N} \sum_{j=1}^{N} \left[e^{\lambda^{(j)}+\frac{\tau^{(j)2}}{2}} \Phi(\tau^{(j)} - \boldsymbol{\beta}^{(j)}) \right]^2 - \hat{P}_F^2(\boldsymbol{\theta}) \right\} \tag{25}$$

$$Cov\left[\hat{P}_F(\boldsymbol{\theta})\right] \approx \frac{\sqrt{Var[\hat{P}_F(\boldsymbol{\theta})]}}{\hat{P}_F(\boldsymbol{\theta})} \tag{26}$$

It can be seen that the FPF is estimated and expressed as a function of samples generated by only a single implementation of Line Sampling with $f(\boldsymbol{x}|\boldsymbol{\theta}^*)$. In this way, repeated reliability analyses are avoided, thus a high computational efficiency is obtained by the Augmented Line Sampling approach. The details of the Augmented Line Sampling procedure can be found in [26, 27].

3.2. Sequential optimization framework

In order to ensure the convergence of the optimization process, the sequential optimization framework [1, 28] is adopted to cooperate with the Augmented Line Sampling approach. Then, the Augmented Line Sampling and deterministic optimization are performed iteratively, producing a series of candidates that converge to the optimal solution.

Suppose the number of the current iteration is K, with $K = 1, 2, \ldots$. In this iteration, Augmented Line Sampling is applied to obtain the FPF with an updated instrumental PDF given by

$$f(\boldsymbol{x}|\boldsymbol{\theta}^*) = f(\boldsymbol{x} \mid \boldsymbol{\theta}_{\text{opt}}^{(K-1)}), \tag{27}$$

where $\boldsymbol{\theta}_{\text{opt}}^{(K-1)}$ is the candidate solution in the $(K-1)^{th}$ iteration. Note that $\boldsymbol{\theta}_{\text{opt}}^{(0)}$ is the initial design. As such, the important direction $\boldsymbol{\alpha}^{(K)}$ is also updated as

$$\boldsymbol{\alpha}^{(K)} = \frac{T_{xu}(\boldsymbol{x}^{*(K)} \mid \boldsymbol{\theta}_{\text{opt}}^{(K-1)})}{||T_{xu}(\boldsymbol{x}^{*(K)} \mid \boldsymbol{\theta}_{\text{opt}}^{(K-1)})||}, \tag{28}$$

where $\boldsymbol{x}^{*(K)}$ is the design point solved in the K^{th} iteration, corresponding to the case where $\boldsymbol{x}$ is distributed as $f(\boldsymbol{x} \mid \boldsymbol{\theta}_{\text{opt}}^{(K-1)})$. As a result of carrying out Line Sampling with $f(\boldsymbol{x} \mid \boldsymbol{\theta}_{\text{opt}}^{(K-1)})$, a number of $N^{(K)}$ samples are obtained, i.e., $\left\{\boldsymbol{u}^{\perp(j)} : j = 1, \cdots, N^{(K)}\right\}$. Then, the unbiased estimate of FPF $\hat{P}_F^{(K)}(\boldsymbol{\theta})$ in the K^{th} iteration can be obtained according to Eq. (24), which is:

$$\hat{P}_F^{(K)}(\boldsymbol{\theta}) = \frac{1}{N^{(K)}} \sum_{j=1}^{N^{(K)}} \Phi\left[e^{\lambda^{(j)} + \frac{\tau^{(j)2}}{2}} \Phi(\tau^{(j)} - \boldsymbol{\beta}^{(j)})\right]. \tag{29}$$

After the FPF estimate is obtained in Eq. (29), it can be substituted into the original RBDO problem in Eq. (1), transforming it to a equivalent deterministic one. Note that this estimate is a local approximation around the reference point $\boldsymbol{\theta}_{\text{opt}}^{(K-1)}$. Considering this, it is more reasonable to solve the optimization problem in a relatively small sub-domain instead of the original one. Thus, the original optimization problem in Eq. (1) is cast as:

$$\begin{aligned} \text{Min} \quad & W(\boldsymbol{\theta}) \\ \text{s.t.} \quad & \hat{P}_F^{(K)}(\boldsymbol{\theta}) \leq P_{Fl}^{\text{tol}} \\ & C_j(\boldsymbol{\theta}) \leq 0 \qquad (j = 1, 2, \ldots, n_C) \\ & \underline{\boldsymbol{\theta}}^{(K)} \leq \boldsymbol{\theta} \leq \overline{\boldsymbol{\theta}}^{(K)} \quad . \end{aligned} \tag{30}$$

where $\Theta^{(K)} = \left[\underline{\boldsymbol{\theta}}^{(K)}, \overline{\boldsymbol{\theta}}^{(K)}\right]$ is the subdomain associated with the K^{th} iteration. Note that a proper selection of the subdomain is important for the efficiency of the proposed approach. The sequence of search domains for optimization $\Theta^{(K)}$ can be selected as [1, 11]:

$$\begin{aligned} \underline{\boldsymbol{\theta}}^{(K)} &= \max\left\{\boldsymbol{\theta}_{\text{opt}}^{(K-1)} - R_K|\boldsymbol{\theta}_{\text{opt}}^{(K-1)}|, \underline{\boldsymbol{\theta}}\right\}, \\ \overline{\boldsymbol{\theta}}^{(K)} &= \min\left\{\boldsymbol{\theta}_{\text{opt}}^{(K-1)} + R_K|\boldsymbol{\theta}_{\text{opt}}^{(K-1)}|, \overline{\boldsymbol{\theta}}\right\}, \end{aligned} \tag{31}$$

where R_K is the factor that determines the size of the local optimization domain. A gradual change strategy for $R_K = R_0 \times r^K$ can be set where R_0 is initial value, e.g., R_0 can be chosen between 10% and 50%, and r is reduction factor within the range of $[0.8, 1]$. This gradual change strategy is adopted to determine a new subdomain for identifying a candidate optimal design for next step. Note that large R_0 can be selected if an accurate estimator of FPF can be obtained, and vice versa. For example, when the C.o.V. of the obtained FPF estimate at the current optimal design, i.e, $Cov[\hat{P}_F^{(K)}(\boldsymbol{\theta}_{\text{opt}}^{(K-1)})]$, is smaller than 0.2, then $R_0 = 20\%$ and $r = 0.9$ is suitable, otherwise $R_0 = 10\%$ and $r = 0.95$ may be better.

Solving this deterministic optimization in the subdomain produces a new candidate solution $\boldsymbol{\theta}_{\text{opt}}^{(K)}$. Note that in Eq. (31), $\hat{P}_F^{(K)}(\boldsymbol{\theta})$ is available as an explicit function of the design variables. As such, any optimization algorithm can be employed in the minimization procedure without additional (expensive) evaluations of the performance function.

In this way, rather than solving the RBDO problem by solving the nested double loop optimization, the RBDO in this contribution is reduced to iteratively solving a deterministic optimization problem in a subdomain, along with obtaining the FPF estimation for replacing the probabilistic constraint of RBDO. The latter demands carrying out a single reliability analysis in augmented space per iteration of the sequential optimization scheme.

3.3. Combination algorithm

To aggregate the information of all iterations up to the current one, a combination algorithm is implemented [29, 30]. This algorithm is based on the weighted sum of the local FPF estimators until iteration K. It aims at reusing the information of the $k = 1, \ldots, K$ iterations in the K^{th} iteration, to improve the efficiency for obtaining an accurate FPF estimate. Specifically, the FPF is cast as:

$$\hat{P}_{F,C}^{(K)}(\boldsymbol{\theta}) = \sum_{k=1}^{K} w_k(\boldsymbol{\theta}) \hat{P}_F^{(k)}(\boldsymbol{\theta}), \tag{32}$$

where $w_k(\boldsymbol{\theta})$ is the weight function. To ensure that $\hat{P}_{F,C}^{(K)}(\boldsymbol{\theta})$ is unbiased, $\sum_{k=1}^{K} w_k(\boldsymbol{\theta}) = 1$ is imposed for each value of $\boldsymbol{\theta}$. Note that, as $\hat{P}_F^{(K)}(\boldsymbol{\theta})$ is unbiased, thus the obtained $\hat{P}_{F,C}^{(K)}(\boldsymbol{\theta})$ is also unbiased.

The performance of the combination algorithm is quite dependent on the weights, and as a consequence, dependent on which principle is used to determine the weights. In this contribution, three possible ways are explored: (1) equal weights; (2) weight w_k that minimizes the variance of $\hat{P}_{F,C}^{(K)}(\boldsymbol{\theta})$; and (3) weight w_k that minimizes the C.o.V. of $\hat{P}_{F,C}^{(K)}(\boldsymbol{\theta})$. These three alternatives have been explored in [31], where it is shown that the last one is most effective and stable and hence, it is adopted here. Indeed, imposing that $\hat{P}_{F,C}^{(K)}(\boldsymbol{\theta})$ possesses the smallest possible C.o.V., the optimal weights are determined as follows. First, as $\hat{P}_F^{(k)}(\boldsymbol{\theta})(k = 1, \ldots, K)$ given in Eq. (29)

is unbiased, i.e., $E[\hat{P}_F^{(k)}(\boldsymbol{\theta})] = P_F(\boldsymbol{\theta})$, the C.o.V. of the estimate of FPF, $Cov[\hat{P}_{F,C}^{(K)}(\boldsymbol{\theta})]$, is:

$$Cov[\hat{P}_{F,C}^{(K)}(\boldsymbol{\theta})] = \frac{\sqrt{\sum_{k=1}^{K} w_k^2(\boldsymbol{\theta}) Var[\hat{P}_F^{(k)}(\boldsymbol{\theta})]}}{P_F(\boldsymbol{\theta})} = \sqrt{\sum_{k=1}^{K} w_k^2(\boldsymbol{\theta}) Cov^2[\hat{P}_F^{(k)}(\boldsymbol{\theta})]} \tag{33}$$

As the optimization problem of minimizing the $Cov[\hat{P}_{F,C}^{k}(\boldsymbol{\theta})]$ is equal to minimizing the $Cov^2[\hat{P}_{F,C}^{k}(\boldsymbol{\theta})]$, then the optimal weights based on minimizing the C.o.V. can be determined by solving the following optimization problem:

$$\begin{aligned} \min \quad & Cov^2[\hat{P}_{F,C}^{k}(\boldsymbol{\theta})] = \sum_{k=1}^{K} w_k^2(\boldsymbol{\theta}) Cov^2\left[\hat{P}_F^{(k)}(\boldsymbol{\theta})\right] \\ s.t. \quad & \sum_{k=1}^{K} w_k(\boldsymbol{\theta}) = 1 \end{aligned} \tag{34}$$

The Lagrangian of the problem in Eq. (34) is:

$$L(\boldsymbol{w}, \lambda) = \sum_{k=1}^{K} w_k^2(\boldsymbol{\theta}) Cov^2\left[\hat{P}_F^{(k)}(\boldsymbol{\theta})\right] + \lambda\left(\sum_{k=1}^{K} w_k(\boldsymbol{\theta}) - 1\right) \tag{35}$$

The first-order necessary optimality conditions read:

$$\begin{aligned} \frac{\partial L(\boldsymbol{w}, \lambda)}{\partial w_k(\boldsymbol{\theta})} &= 0 \\ \frac{\partial L(\boldsymbol{w}, \lambda)}{\partial \lambda} &= 0 \end{aligned} \tag{36}$$

Solving this equation will result in the following expressions

$$\begin{aligned} w_k(\boldsymbol{\theta}) &= -\frac{\lambda}{2} Cov^{-2}\left[\hat{P}_F^{(k)}(\boldsymbol{\theta})\right] \\ \lambda &= -\frac{2}{\sum_{k=1}^{K} Cov^{-2}\left[\hat{P}_F^{(k)}(\boldsymbol{\theta})\right]} \end{aligned} \tag{37}$$

and finally, it gives the optimal weights that minimise the C.o.V.:

$$w_k^c(\boldsymbol{\theta}) = \frac{Cov^{-2}\left[\hat{P}_F^{(k)}(\boldsymbol{\theta})\right]}{\sum_{j=1}^{k} Cov^{-2}\left[\hat{P}_F^{(j)}(\boldsymbol{\theta})\right]} \quad (k = 1, \cdots, K) \tag{38}$$

Since the objective function is convex (quadratic in w) and the constraint is affine, the result of Eq. (38) is the global optimum.

Similarly, the optimal weights that minimise the variance, $w_i^v(\boldsymbol{\theta})$, can be also obtained by

$$w_i^v(\boldsymbol{\theta}) = \frac{Var^{-1}\left[\hat{P}_F^{(k)}(\boldsymbol{\theta})\right]}{\sum_{j=1}^{K} Var^{-1}\left[\hat{P}_F^{(j)}(\boldsymbol{\theta})\right]} \quad (k = 1, \cdots, K) \tag{39}$$

In addition, the average (equal) weights, $w_i^a(\boldsymbol{\theta})$, are equal to:

$$w_k^a(\boldsymbol{\theta}) = \frac{1}{K} \quad (k = 1, \cdots, K) \tag{40}$$

3.4. Decoupling the RBDO by using combination FPF

After the combined FPF estimator with respect to design variables, $\hat{P}_{F,C}^{(K)}(\boldsymbol{\theta})(K > 1)$, has been obtained according to Eq. (32), the RBDO can be decoupled in the $K^{th}(K > 1)$ iteration as

$$\begin{aligned} \text{Min} \quad & W(\boldsymbol{\theta}) \\ \text{s.t.} \quad & \hat{P}_{F,C}^{(K)}(\boldsymbol{\theta}) \leq P_F^{\text{tol}} \\ & C_j(\boldsymbol{\theta}) \leq 0 \qquad (j = 1, 2, \ldots, n_C) \\ & \underline{\boldsymbol{\theta}}^{(K)} \leq \boldsymbol{\theta} \leq \bar{\boldsymbol{\theta}}^{(K)} \quad . \end{aligned} \tag{41}$$

Solving this optimization problem in Eq. (41) produces a new candidate solution $\boldsymbol{\theta}_{\text{opt}}^{(K)}$. As the estimate $\hat{P}_{F,C}^{(K)}(\boldsymbol{\theta})$ is merely a function of samples (closed-form), any optimization algorithm can be adopted to solve the optimization problem. Note that no additional evaluations of performance function are involved.

3.5. Procedure of the proposed approach

Fig. 1 shows the procedure of the proposed strategy to solve the RBDO problem, which can be summarized as follows.

1. Initialize the design parameters $\boldsymbol{\theta}_{\text{opt}}^{(0)}$.
   The initial design $\boldsymbol{\theta}_{\text{opt}}^{(0)}$ can be arbitrarily selected from the design domain Θ. Set $K = 1$.
2. Carry out Augmented Line Sampling.
   Based on the former solution $\boldsymbol{\theta}_{\text{opt}}^{(K-1)}$, carry out Line Sampling with $f(\boldsymbol{x}|\boldsymbol{\theta}_{\text{opt}}^{(K-1)})$.
3. Obtain the FPF estimator.
   Obtain the FPF $\hat{P}_F^{(K)}(\boldsymbol{\theta})$ according to Eq. (29) in the current K-th iteration. And then the combined FPF estimator $\hat{P}_{F,C}^{(K)}(\boldsymbol{\theta})$ is established according to Eq. (32) by using the combination weight approach (either $ALS(w_k^a(\boldsymbol{\theta}))$, $ALS(w_k^v(\boldsymbol{\theta}))$ or $ALS(w_k^c(\boldsymbol{\theta}))$).
4. Decouple the RBDO problem.
   Use the obtained FPF to decouple the RBDO, then carry out the deterministic optimization of Eq. (41) to obtain a new candidate solution $\boldsymbol{\theta}_{\text{opt}}^{(K)}$.
5. Set $K = K + 1$. Repeat steps 2-4, until convergence is reached.

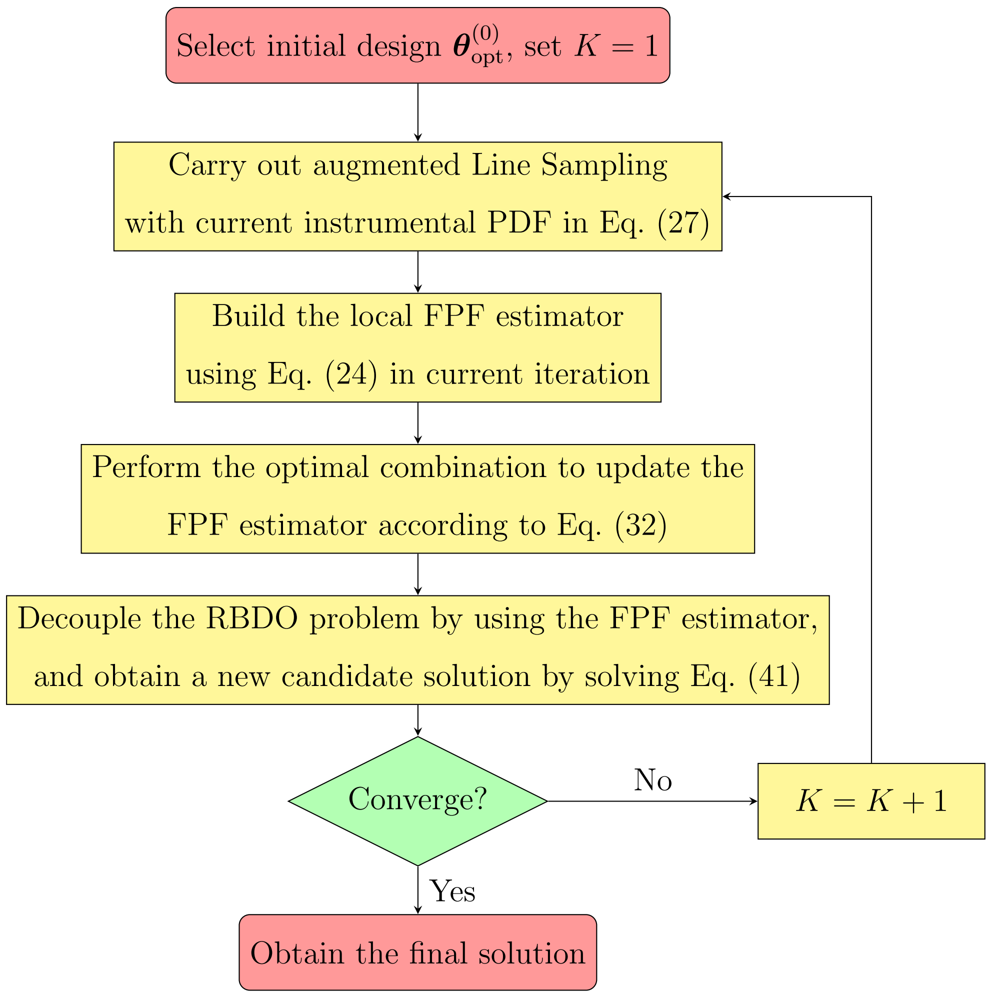

Figure 1: Flowchart of the procedure of the proposed approach.

4. Examples

In this section, four examples are given to illustrate the performance of the proposed approaches. For comparison, four different approaches are adopted to solve these examples:

(a) The proposed approach, as described in Section 3, which includes Augmented Line Sampling (ALS) (see Eq.(30)) and Augmented Line Sampling with combination algorithm (see Eq.(41)).

(b) A decoupling approach proposed in [7] where the logarithm of the FPF is approximated as a linear polynomial (LP). The coefficients of this polynomial are evaluated in a least squares sense by conducting several runs of Line Sampling in the associated local domain. This approach is denoted as 'Decoupling LP'.

(c) An decoupling approach denoted as 'Decoupling QP' where the logarithm of the FPF is approximated by means of a quadratic polynomial (QP), as used in [6].

(d) A double-loop approach taking original Line Sampling as the way of calculating the probabilistic constraint. It is denoted as 'Double-loop LS'.

Note that, the optimization algorithms enclosed in the Matlab R2021a function `fmincon` are used to solve the 'outer' loop of RBDO in the double-loop approach. The function `fmincon` is also used to optimize the decoupled problem when the FPF is estimated by the proposed approach or by the approximation (Decoupling LP or Decoupling QP). The settings for constructing the sub-domain as cast in Eq. (31) are $R_0 = 20\%$ and $\rho = 0.9$ for all examples, which exhibits good performance. The stopping criterion $||(\boldsymbol{\theta}_{\text{opt}}^{(K)} - \boldsymbol{\theta}_{\text{opt}}^{(K-1)})/\boldsymbol{\theta}_{\text{opt}}^{(K-1)}|| \leq \theta_{tol}$ is set where the tolerance value $\theta_{tol} = 2\%$ is used for all the examples.

4.1. Example 1: A roof structure

A roof structure shown in Fig. 2 is considered here, which is revised from [32] to suit the purpose of this paper. The upper chord and compression bars are made of reinforced concrete, and the bottom chord and the tension bars are made of steel. A uniformly distributed load q is applied on the roof truss, which is transformed into a nodal load $P = ql/4$ where l is the length of the roof. Failure is defined as the vertical deflection of the structure's node C exceeding $\Delta = 0.05$m, and the corresponding limit state function is given as

$$g(\boldsymbol{x}) = \Delta - \frac{ql^2}{2}\left(\frac{3.81}{A_C E_C} + \frac{1.13}{A_S E_S}\right), \tag{42}$$

where E_S and E_C are the elastic modulus of steel and concrete; A_S and A_C are sectional areas related to steel and concrete parts, respectively. The distribution information of the basic random variables is given in Table 1. It is assumed that all variables follow a normal distribution and truncation is applied over those parameters which admit positive values due to physical reasons.

Two design parameters are considered in this example, $\boldsymbol{\theta} = [\mu_{A_S}, \mu_{A_C}]$, which are the mean values of A_S and A_C. Their corresponding design domains are $\theta_1 \in [8, 12] \times 10^{-4}$ m^2 and $\theta_2 \in [0.03, 0.05]$ m^2, respectively. The corresponding RBDO problem is

$$\begin{aligned} \min_{\boldsymbol{\theta}} \quad & W(\boldsymbol{\theta}) = 3.1112\theta_1 + 1.1859\theta_2 \\ \text{s.t.} \quad & P_F(\boldsymbol{\theta}) \leq 10^{-4} \\ & 8 \times 10^{-4} \leq \theta_1 \leq 12 \times 10^{-4} \\ & 0.03 \leq \theta_2 \leq 0.05, \end{aligned} \tag{43}$$

where the objective function $W(\boldsymbol{\theta})$ is related to the cost of the roof, which refers to the volume; and the probabilistic constraint $P_F(\boldsymbol{\theta})$ is the failure probability function, which should be equal or smaller than 10^{-4}.

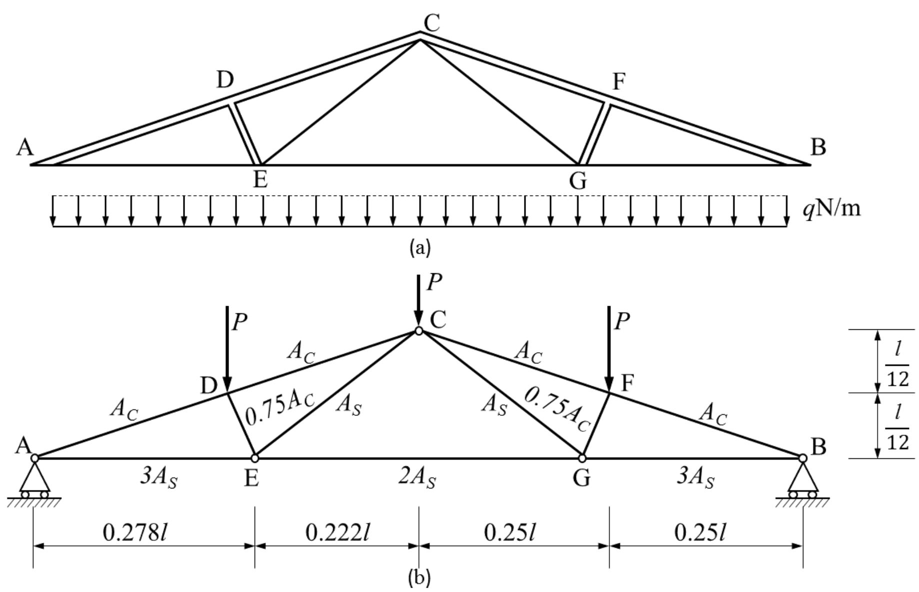

Figure 2: The sketch of roof truss.

4.1.1. Comparison of combination alternatives

The proposed approaches (ALS, $ALS(w_k^a(\boldsymbol{\theta}))$, $ALS(w_k^v(\boldsymbol{\theta}))$, $ALS(w_k^c(\boldsymbol{\theta}))$) are applied to solve this RBDO problem. For each approach, the same initial point is used which is selected as the upper bounds of the design interval: $\boldsymbol{\theta}_{\text{opt}}^{(0)} = [1.2 \times 10^{-4}, 0.05]$.

Table 1: The distribution information of the basic random variables (Example 1).

Random variable	$A_S(\mathrm{m}^2)$	$A_c(\mathrm{m}^2)$	$E_S(\mathrm{N/m}^2)$	$E_C(\mathrm{N/m}^2)$	$q(\mathrm{N/m})$	$l(\mathrm{m})$
Mean value	$\theta = \mu_{As}$	$\theta = \mu_{Ac}$	1×10^{11}	2×10^{10}	20,000	12
Standard deviation	9.82×10^{-5}	0.004	1×10^{10}	2×10^{9}	2000	0.12

Fig. 3 shows the results of the objective function, the number of iterations, the FPF estimates as well as their C.o.V's with respect to the number of samples $N^{(K)}$ obtained by the proposed method, where $N^{(K)}$ is varied between 100 and 1000. The 'Exact' value refers to the result obtained by 'Decoupling LS' with 1000 samples for each LS run, which is also listed in Table 2. It can be seen from the figure that, $ALS(w_k^v(\boldsymbol{\theta}))$ and $ALS(w_k^c(\boldsymbol{\theta}))$ can converge in less than 5 iterations when different number of samples are used. While ALS and $ALS(w_k^a(\boldsymbol{\theta}))$ show some variations, e.g. almost 10 iterations are required by $ALS(w_k^a(\boldsymbol{\theta}))$ when $N^{(K)} = 900$.

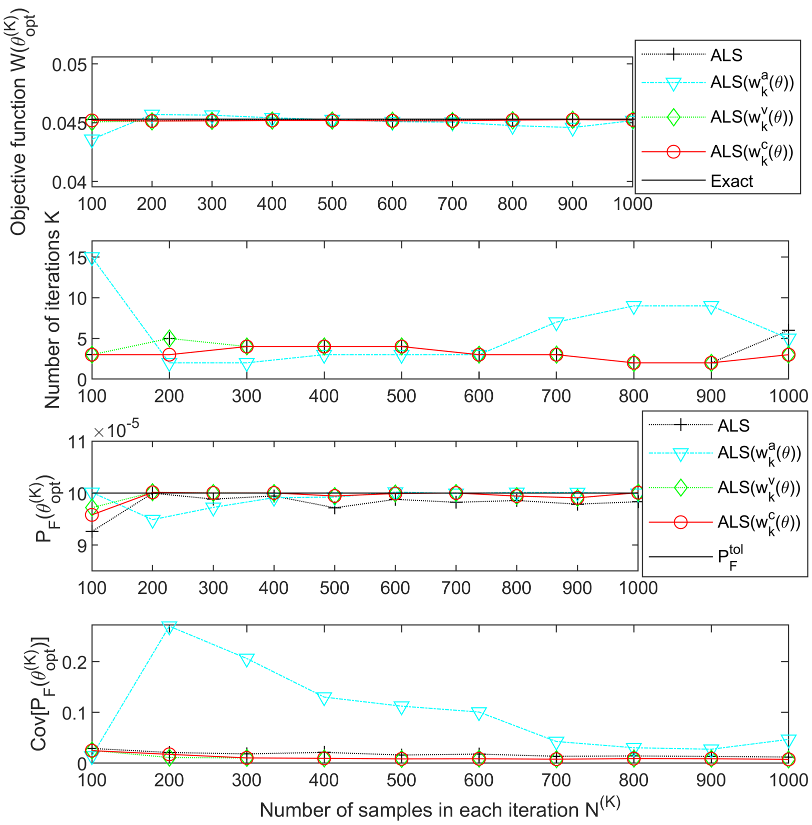

Figure 3: Evolution of different results with respect to the number of samples ($N^{(K)}$) employing the proposed approaches (Example 1).

For demonstration purposes, Figs. 4a and 4b show respectively the one-dimensional FPF for $P_F(\theta_1, \theta_2 = 0.04)$ and $P_F(\theta_1 = 1.0 \times 10^{-4}, \theta_2)$ corresponding to the $K = 2^{nd}$ iteration with $N^{(K)} = 400$. The point-wise failure probability results by adopting direct MCS with 10^7 samples for each are taken as the 'Exact' values which are shown by dots in the figures. It can be seen from the figure that the estimates of FPF obtained by ALS in each iteration have some error over some regions. For example, when $\theta_1 \in [0.8, 1.0] \times 10^{-4}$ which is a little far from $\boldsymbol{\theta}_{\text{opt}}^{(0)} = [1.2 \times 10^{-4}, 0.05]$ m^2, the obtained FPF estimators by ALS shows considerable error and the corresponding C.o.V. is relatively large (see Fig. 4a). Similar phenomena can be seen in Fig. 4b. The reason is that the FPF estimated by ALS is valid over small region (that is, it is a local estimate). When $\boldsymbol{\theta}$ is far from $\boldsymbol{\theta}_{\text{opt}}^{(K-1}$, the implementation of ALS based on $\boldsymbol{\theta}_{\text{opt}}^{(K-1)}$ may fail in inferring the failure probability value corresponding to $\boldsymbol{\theta}$, leading to a bigger C.o.V. of FPF. Further, it can also be seen that the combination algorithm may alleviate these issues by integrating multiple FPF estimators. As in the second iteration, a relatively accurate FPF estimate can be obtained by using the proposed combination algorithm with the different weight functions ($ALS(w_k^a(\boldsymbol{\theta}))$, $ALS(w_k^v(\boldsymbol{\theta}))$ and $ALS(w_k^c(\boldsymbol{\theta}))$). However, among these combination ways, the result of $w_k^v(\boldsymbol{\theta})$ still has significant error at the tail of the design region, for example, when $\theta_1 \in [0.8, 0.9] \times 10^{-4}$ m^2 by $ALS(w_k^v(\boldsymbol{\theta}))$ in Fig. 4a. The proposed combination based on $w_k^c(\boldsymbol{\theta})$ obtains the most accurate FPF results. The advantage of using $w_k^c(\boldsymbol{\theta})$ as weights in the combination algorithm has been shown by Figs. 3 and 4.

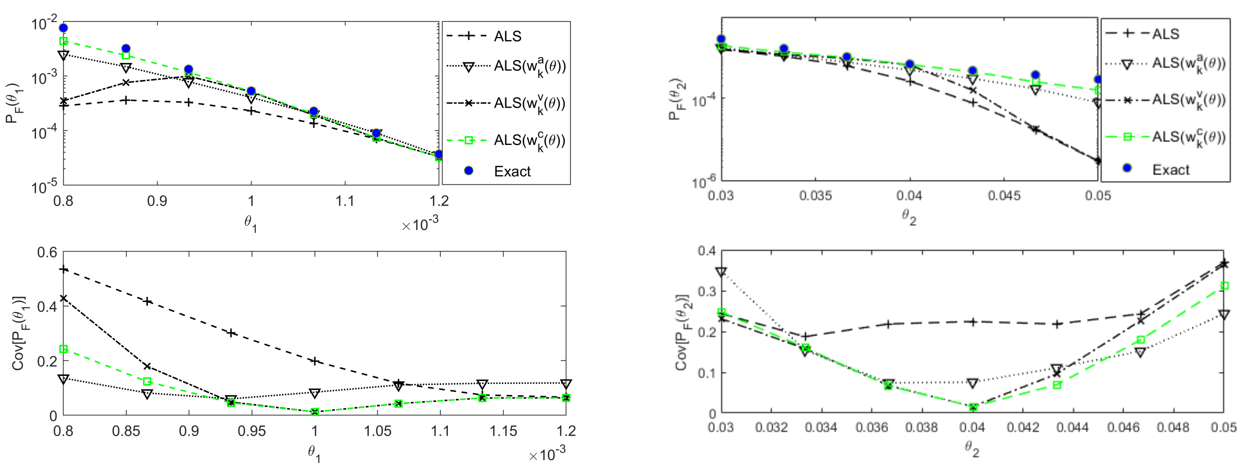

(a) $P_F(\theta_1, \theta_2 = 0.04)$ (b) $P_F(\theta_1 = 1.0 \times 10^{-4}, \theta_2)$

Figure 4: The FPF estimation in $K = 2$ -th iteration by different approaches (Example 1).

4.1.2. Comparison with other Methods

The proposed approach is compared with other RBDO approaches present in literature, i.e., Decoupling LP, Decoupling QP, and Double-loop LS. For the reliability part, Line Sampling with $N = 400$ samples is adopted in each sequential optimization iteration to solve the RBDO problem. For comparison, Line Sampling with the same number of samples is used in the other methods. The result of Double-loop LS with $N = 1000$ is taken as the 'exact' value.

The results by different methods as well as the corresponding computational cost are listed in Table 2. Specifically, the values of the constraint at the final optimal solution, as well as their C.o.V.'s are shown in the Table. The computational cost for each method is also given. Note that the value of constraint (failure probability $P_F(\boldsymbol{\theta}_{\text{opt}}^{(K)})$) is computed by carrying out one more run of ALS to check the 'real' value, which is estimated by $\hat{P}_F^{(K+1)}(\boldsymbol{\theta}_{\text{opt}}^{(K)})$, but not the inferred value, i.e., $P_F^{(K)}(\boldsymbol{\theta}_{\text{opt}}^{(K)})$. For the compared decoupling methods (decoupling LP and QP), one more reliability is also carried out to calculate the failure probability corresponding to $\boldsymbol{\theta}_{\text{opt}}^{(K)}$. Concerning the computation cost, as mentioned above, only one reliability analysis (Line Sampling here) in the proposed approach is required to obtain the estimation of the FPF, while for Decoupled LP, $n_\theta + 1 = 3$ times of Line Sampling analyses are needed, and $2n_\theta + 1 = 5$ times for Decoupled QP. It can be seen that the results of different methods are quite consistent with each other. Among them, the proposed approaches (ALS, $ALS(w_k^a(\boldsymbol{\theta}))$, $ALS(w_k^v(\boldsymbol{\theta}))$ and $ALS(w_k^c(\boldsymbol{\theta}))$) obtain satisfactory results with less number of samples than other methods.

Table 2: Results of optimization by different approaches (Example 1)

	$W(\boldsymbol{\theta}_{\text{opt}}^{(K)})$	$P_F(\boldsymbol{\theta}_{\text{opt}}^{(K)})$(C.o.V.)	$\boldsymbol{\theta}_{\text{opt}}^{(K)}(\times 10^{-2})$	$K \times N^{(K)}$
ALS	4.52×10^{-2}	$9.9 \times 10^{-5}(0.02)$	$[0.12, 3.50]$	4×400
ALS-$w_k^a(\boldsymbol{\theta})$	4.54×10^{-2}	$9.9 \times 10^{-5}(0.13)$	$[0.12, 3.52]$	3×400
ALS-$w_k^v(\boldsymbol{\theta})$	4.52×10^{-2}	$1.0 \times 10^{-4}(0.01)$	$[0.12, 3.50]$	4×400
ALS-$w_k^c(\boldsymbol{\theta})$	4.52×10^{-2}	$1.0 \times 10^{-4}(0.01)$	$[0.12, 3.50]$	4×400
Decoupling LP	4.53×10^{-2}	$1.0 \times 10^{-4}(0.02)$	$[0.12, 3.50]$	$4 \times (3 \times 400)^{\#}$
Decoupling QP	4.53×10^{-2}	$1.0 \times 10^{-4}(0.02)$	$[0.12, 3.50]$	$4 \times (5 \times 400)$
Double-loop LS	4.53×10^{-2}	$1.0 \times 10^{-4}(0.02)$	$[0.12, 3.50]$	33×400
Double-loop LS	4.53×10^{-2}	$1.0 \times 10^{-4}(0.01)$	$[0.12, 3.50]$	45×1000

#Values in parentheses is the number of runs of LS multiplied by the number of samples in each run.

4.1.3. *Performance with respect to different initial designs*

To illustrate the robustness of the method, the optimization is started with different initial design settings, i.e.,

- $\boldsymbol{\theta}_{\text{opt}}^{(0)} = [0.12, 5] \times 10^{-2}$ which is the upper bound of the design region (denoted as Case A).
- $\boldsymbol{\theta}_{\text{opt}}^{(0)} = [0.10, 4] \times 10^{-2}$ which is the midpoint of the design region (denoted as Case B);
- $\boldsymbol{\theta}_{\text{opt}}^{(0)} = [0.08, 3] \times 10^{-2}$ which is the lower bound of the design region (denoted as Case C).

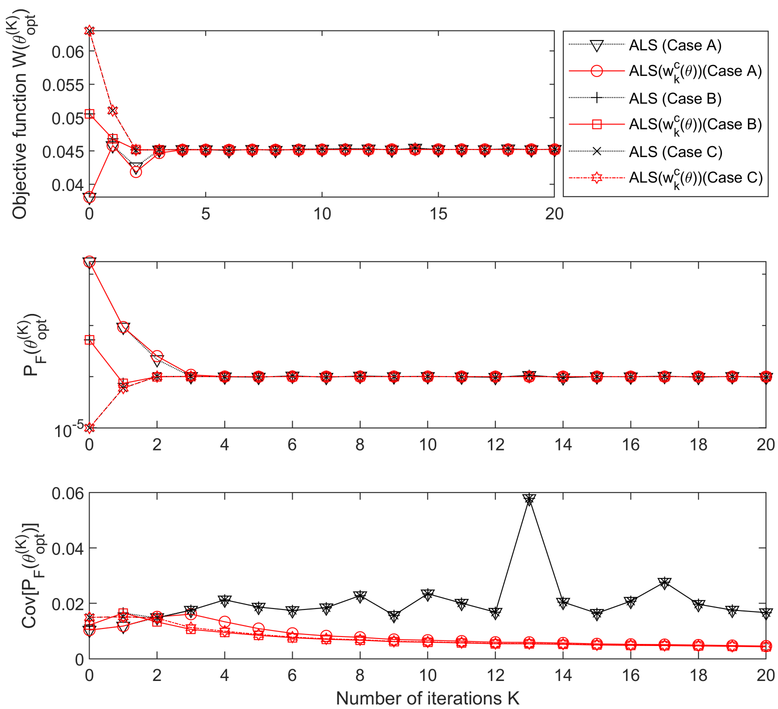

Figure 5: Evolution of the objective function and failure probability by the proposed approach for a given number of iterations K (Example 1).

Fig. 5 shows the evolution of the objective function and FPF estimates by ALS and ALS based on a combination with $w_k^c(\boldsymbol{\theta})$(as well as the corresponding C.o.V.'s) with respect to the number of iterations. It is can be seen from the figure that, no matter which initial design is used, the combination algorithm based on the weights $w_k^c(\boldsymbol{\theta})$ can obtain more accurate FPF estimators, as shown by the lower C.ov. values.

4.2. Example 2: A front axle

This example considers the front axle of a car, which is a crucial component for the structural reliability [33]. Fig. 6 shows an illustration of the cross-section of a typical front axle.

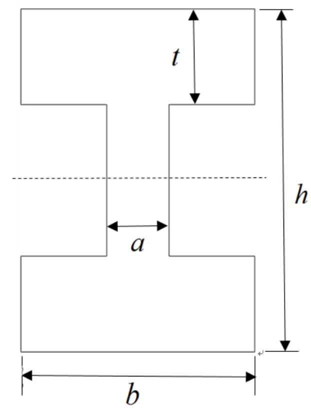

Figure 6: Diagram of automobile front axle.

Considering the static strength of the front axle, the limit-state function is expressed as

$$g(\boldsymbol{x}) = [\sigma] - \sqrt{\sigma_n^2(\boldsymbol{x}) + 3\tau_S^2(\boldsymbol{x})}, \tag{44}$$

where $\boldsymbol{x} = [a, t, b, h, M, T]$ is the vector of random variables; $[\sigma]$ is the yield stress, which is set to 680 MPa according to the material specifications of the front axle. The normal stress and shear stress are $\sigma_n(\boldsymbol{x}) = M/W_s(\boldsymbol{x})$ and $\tau_S(\boldsymbol{x}) = T/W_\rho(\boldsymbol{x})$, where M and T are bending moment and torque, respectively, $W_s(\boldsymbol{x})$ and $W_\rho(\boldsymbol{x})$ are section factor and polar section factor, respectively, which are given as:

$$W_s(\boldsymbol{x}) = \frac{a(h-2t)^3}{6h} + \frac{b}{6h}\left[h^3 - (h-2t)^3\right] \tag{45}$$

$$W_\rho(\boldsymbol{x}) = 0.8bt^2 + 0.4\left[a^3(h-2t)/t\right] \tag{46}$$

Table 3 lists the distribution information of the basic random vairables, where the geometric variables of the beam, i.e., t, h, a, b are normal variables and the loads T and M are Log-normal variables. Due to physical reasons, all the variables are restricted to positive values. Four design parameters are included in this example, $\boldsymbol{\theta} = [\mu_a, \mu_t, \mu_b, \mu_h]$, which are the mean values of a, t, b and h. Their corresponding design domains are $\theta_1 = \mu_a \in [10, 14], \theta_2 = \mu_t \in [12, 16], \theta_3 = \mu_b \in$

$[60, 70]$ and $\theta_4 = \mu_h \in [80, 90]$, respectively. The corresponding RBDO problem is

$$\begin{aligned} \min_{\boldsymbol{\theta}} \quad & W(\boldsymbol{\theta}) = \theta_1\theta_4 + 2\left(\theta_3 - \theta_1\right)\theta_2 \\ \text{s.t.} \quad & P_F(\boldsymbol{\theta}) \leq 10^{-3} \\ & 10 \leq \theta_1 \leq 14, 12 \leq \theta_2 \leq 16 \\ & 60 \leq \theta_3 \leq 70, 80 \leq \theta_4 \leq 90, \end{aligned} \tag{47}$$

where the objective function $W(\boldsymbol{\theta})$ is related to the cost of the front axle, which refers to the cross sectional area; and the probabilistic constraint is the failure probability function, which should be equal or smaller than 10^{-3}.

Table 3: The distribution information of the random variables in Example 2

Random variable	a(mm)	t(mm)	b(mm)	h(mm)	$T(\text{kN}\cdot\text{m})$	$M(\text{kN}\cdot\text{m})$
Mean value	$\theta_1 \in [10, 14]$	$\theta_2 \in [12, 16]$	$\theta_3 \in [60, 70]$	$\theta_4 \in [80, 90]$	3.1	3.5
Standard deviation	1.2	1.4	6.5	8.5	0.31	0.35
Distribution	Normal	Normal	Normal	Normal	Log-Normal	Log-Normal

Table 4: Results of optimization by different approaches (Example 2)

	$W(\boldsymbol{\theta}_{\text{opt}}^{(K)})$	$P_F(\boldsymbol{\theta}_{\text{opt}}^{(K)})$(C.o.V.)	$\boldsymbol{\theta}_{\text{opt}}^{(K)}$	$K \times N^{(K)}$
ALS	9.60×10^2	$9.4 \times 10^{-4}(0.024)$	$[14.00, 12.00, 70.00, 88.55]$	6×400
$ALS(w_k^a(\boldsymbol{\theta}))$	9.66×10^2	$9.9 \times 10^{-4}(0.058)$	$[14.00, 12.00, 70.00, 88.99]$	4×400
$ALS(w_k^v(\boldsymbol{\theta}))$	9.53×10^2	$9.9 \times 10^{-4}(0.016)$	$[14.00, 12.00, 70.00, 88.10]$	4×400
$ALS(w_k^c(\boldsymbol{\theta}))$	9.63×10^2	$9.7 \times 10^{-4}(0.015)$	$[14.00, 12.00, 70.00, 88.77]$	4×400
Decoupling LP	9.71×10^2	$9.9 \times 10^{-4}(0.024)$	$[14.00, 12.94, 70.00, 80.00]$	$3 \times (5 \times 400)$
Decoupling QP	9.58×10^2	$1.0 \times 10^{-3}(0.024)$	$[14.00, 12.00, 70.00, 88.43]$	$3 \times (9 \times 400)$
Double-loop LS	9.58×10^3	$1.0 \times 10^{-4}(0.024)$	$[14.00, 12.00, 70.00, 88.43]$	30×400
Double-loop LS	9.56×10^3	$1.0 \times 10^{-4}(0.015)$	$[14.00, 12.00, 70.00, 88.28]$	30×1000

The proposed approach is implemented to solve this problem involving four design parameters. The results by different methods under a certain setting for the number of samples are listed in Table 4. The proposed approach is applied by carrying out Augmented Line Sampling with $N^{(k)} =$ 400 samples in each sequential optimization iteration to solve the RBDO problem. The initial design vector is first simply chosen as the center of the design interval, i.e., $\boldsymbol{\theta}_{\text{opt}}^{(0)} = [12, 14, 65, 85]$. In each iteration of the sequence optimization, the proposed approach carries out one Line Sampling procedure to obtain the estimation of the FPF. For comparison, the other methods also use the same number of samples($N = 400$) in each of implementation of Line Sampling. Note that in each decoupling iteration, $n_\theta + 1 = 5$ times Line Sampling analyses are needed for Decoupled LP, and $2n_\theta + 1 = 9$ times for Decoupled QP in this example (indicated in the Table). It can be seen that the results are quite consistent with each other. Note further that, from all approaches, the proposed approach is the most efficient.

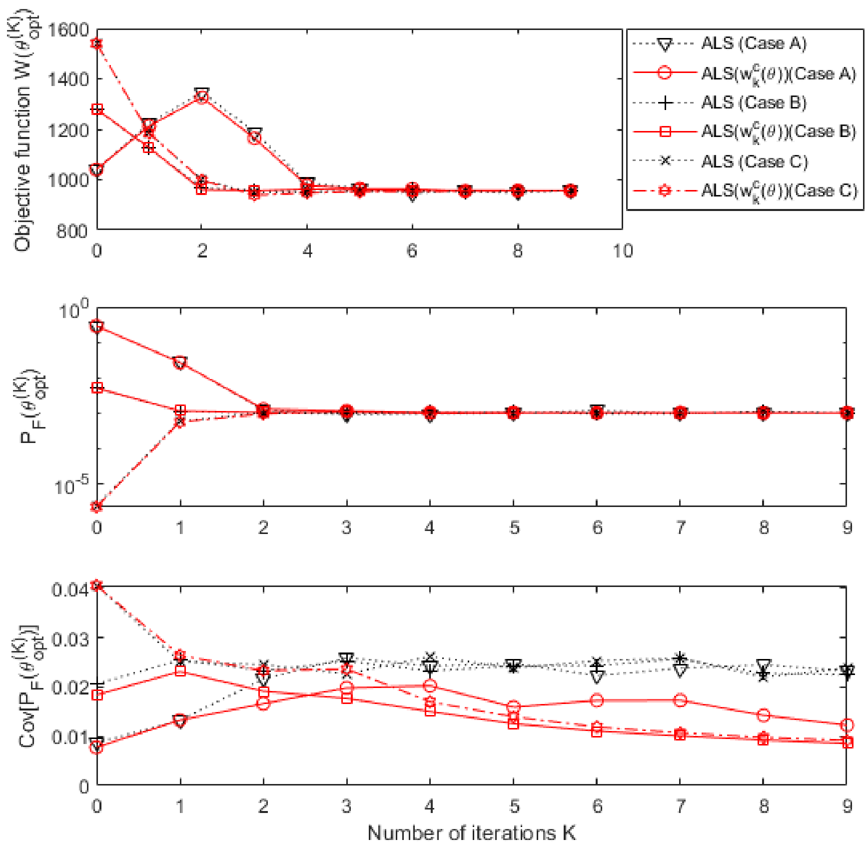

Figure 7: Evolution of the objective function and failure probability by the proposed approach (Example 2).

Next, different initial design settings are set to carry out the optimization i.e.,

- $\boldsymbol{\theta}_{\text{opt}}^{(0)} = [10, 12, 60, 80]$ which is the lower bound of the design region(denoted as Case A).
- $\boldsymbol{\theta}_{\text{opt}}^{(0)} = [12, 14, 65, 85]$ which is the midpoint of the design region (denoted as Case B);
- $\boldsymbol{\theta}_{\text{opt}}^{(0)} = [14, 16, 70, 90]$ which is the upper bound of the design region(denoted as Case C).

Fig. 7 shows the evolution of the objective function and FPF estimates (as well as the corresponding C.o.V.'s) with respect to the number of iterations for a given number of iterations $K = 9$. A similar conclusion can be drawn from the figure that, the proposed combination algorithm based on the weight function $w_k^c(\boldsymbol{\theta})$ can obtain a more accurate FPF estimate (with lowest C.o.V.'s among the tested weighting approaches).

4.3. Example 3: A ten-bar truss

A ten-bar aluminum truss is considered in this example, which corresponds to a modified version of the problem considered in [11]. The truss shown in Fig. 8 is subjected to two vertical loads F_1 and F_2, and a horizontal load F_3. The cross-sectional area of its members is denoted as A_j $(j = 1, 2, \ldots, 10)$, the length of the vertical and horizontal bars L, the modulus of elasticity E are all assumed to be basic random variables following normal distributions (quantities which do not admit negative values are truncated). The performance function is defined as the difference between the vertical displacement δ_2 of joint 2 and the allowable displacement $d_0 = 0.1$, that is:

$$g(\boldsymbol{x}) = d_0 - \delta_2(\boldsymbol{x}), \tag{48}$$

where $\boldsymbol{x} = [A_1, \cdots, A_{10},\ L, E, F_1, F_2, F_3]$ is the vector of basic random variables; $\delta_2(\boldsymbol{x})$ is the actually displacement of joint 2, which can be computed by using a finite element analysis (see Fig. 8). A number of ten design parameters are considered, i.e., $\boldsymbol{\theta} = [\mu_{A_1}, \cdots, \mu_{A_{10}}]$, which are the mean value of $A_i (i = 1, \cdots, 10)$ with the design domains $\theta_i \in [6, 10]$, respectively. The corresponding RBDO problem is

$$\begin{aligned} \min_{\boldsymbol{\theta}} \quad & W(\boldsymbol{\theta}) = \textstyle\sum_{i=1}^{6} \theta_i + \sum_{i=7}^{10} \sqrt{2}\theta_i, \\ \text{s.t.} \quad & P_F(\boldsymbol{\theta}) \leq 10^{-3}, \\ & 6 \leq \theta_i \leq 10, \end{aligned} \tag{49}$$

where the objective function is associated with the cost of the truss, which refers to the volume of material; and the probabilistic constraint $P_F(\boldsymbol{\theta})$ is the failure probability function, which should be equal or smaller than 10^{-3}. The information of basic random variables is given in Table 5.

This example contains n_θ =10 design parameters, which in terms of RBDO is considered to be considerable. The proposed approach is carried out to handle this example with ten design parameters. The initial design is set as $\boldsymbol{\theta}_{\text{opt}}^{(0)} = [8, 8, \ldots, 8]$ which is the midpoint of the design region.

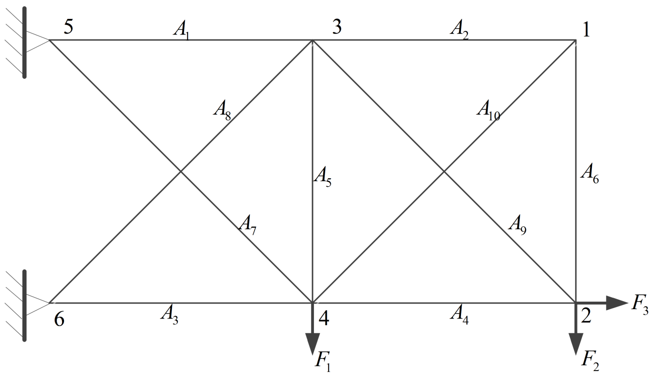

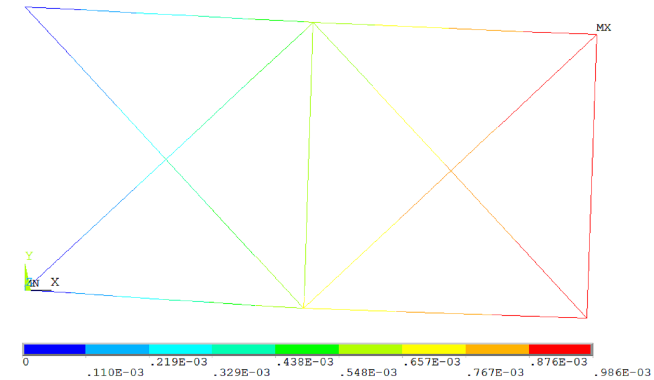

Figure 8: Ten-bar truss structure.

Table 5: Information of variables and parameters for ten-bar truss (Example 3)

Parameter	Distribution	Mean	Standard deviation
$A_1, \cdots, A_{10}$(in)	Normal	$\theta_1, \cdots, \theta_{10}$	0.1
L(in)	Normal	360	3
E(ksi)	Normal	1.5×10^4	1.5×10^2
F_1(kip)	Normal	100	10
F_2(kip)	Normal	120	12
F_3(kip)	Normal	400	40

Fig. 9 shows the results as a function of the number of samples obtained by the proposed approaches (ALS and $ALS(w_k^c(\boldsymbol{\theta}))$). Note that the combination approaches based on $w_k^a(\boldsymbol{\theta})$ and $w_k^v(\boldsymbol{\theta})$ are not included here as they failed to converge within a given maximum number of iterations (30). It can further be seen from the figure that the final optimal solution stays stable for both of the proposed ALS and $ALSw_k^c(\boldsymbol{\theta})$ when the number of samples changes from 200 to 1600. The number of iterations used in the optimization process for ALS, and $ALS(w_k^c(\boldsymbol{\theta}))$ fluctuate for the different $N^{(K)}$, while those of $ALS(w_k^c(\boldsymbol{\theta}))$ exhibit relatively less fluctuation. Meanwhile, the C.o.V.'s of the constraint by ALS in combination with a weighting using $w_k^c(\boldsymbol{\theta})$ are less than those of ALS.

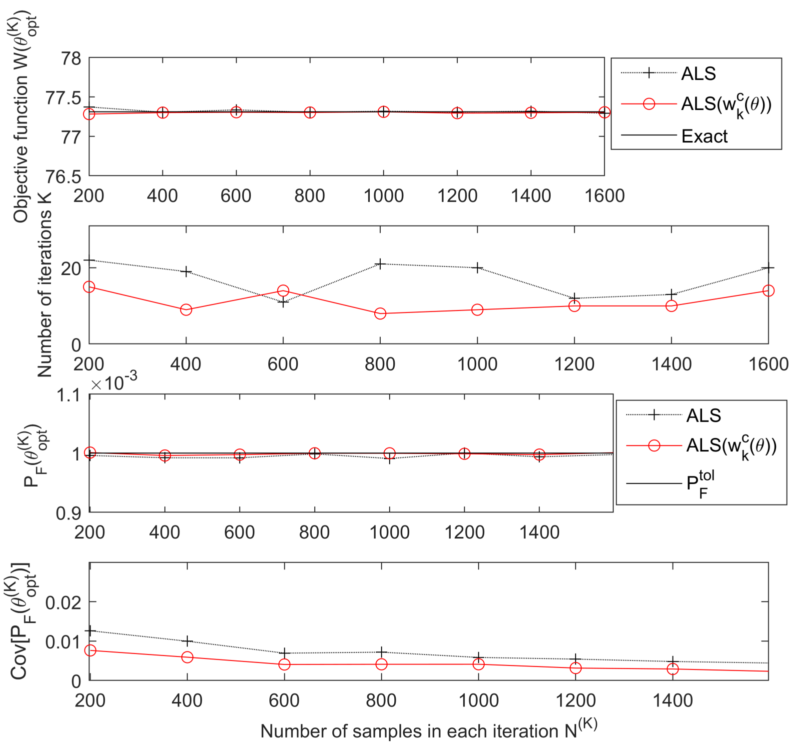

Figure 9: Evolution of different results with respect to the number of samples by the proposed approach (Example 3).

The proposed approaches are also compared with other methods, i.e., Decoupling LP, Decoupling QP, and Double-loop LS. For the reliability analysis part, Line Sampling is adopted with the same number of samples $N = 1000$. The result of another run of Double-loop LS with $N = 3000$ is taken as the exact value. The results by different methods as well as the computational cost are listed in Table 6. It can be seen from the table that the results between different methods are approximately consistent with each other. The proposed approach obtains a satisfied solution with reduced numerical costs. And more specifically, using the proposed weights $w_k^c(\boldsymbol{\theta})$ in the combination algorithm (Eq.(32)) shows a more stable performance with the highest efficiency.

Table 6: Results of optimization by different approaches (Example 3)

	$W(\boldsymbol{\theta}_{\text{opt}}^{(K)})$	$P_F(\boldsymbol{\theta}_{\text{opt}}^{(K)})$(C.o.V.)	$\boldsymbol{\theta}_{\text{opt}}^{(K)}$	$K \times N^{(K)}$
ALS	77.32	$9.9 \times 10^{-4}(0.006)$	$[8.3, 6.0, 9.0, 6.0, 6.0, 6.0, 7.5, 6.0, 6.0, 6.0]$	20×1000
$ALS(w_k^c(\boldsymbol{\theta}))$	77.31	$1.0 \times 10^{-3}(0.005)$	$[8.3, 6.0, 9.0, 6.0, 6.0, 6.0, 7.4, 6.0, 6.0, 6.0]$	9×1000
Decoupling LP	77.36	$1.0 \times 10^{-3}(0.006)$	$[8.5, 6.0, 9.0, 6.0, 6.0, 6.0, 7.2, 6.0, 6.0, 6.0]$	$17 \times (11 \times 1000)$
Decoupling QP	77.31	$1.0 \times 10^{-3}(0.006)$	$[8.2, 6.0, 8.7, 6.0, 6.0, 6.0, 7.7, 6.0, 6.0, 6.0]$	$9 \times (21 \times 1000)$
Double-loop LS	77.31	$1.0 \times 10^{-3}(0.006)$	$[8.2, 6.0, 8.9, 6.0, 6.0, 6.0, 7.6, 6.0, 6.0, 6.0]$	270×1000
Double-loop LS	77.31	$1.0 \times 10^{-3}(0.004)$	$[8.2, 6.0, 8.9, 6.0, 6.0, 6.0, 7.6, 6.0, 6.0, 6.0]$	108×3000

Next, different initial design settings are set to carry out the optimization i.e.,

- $\boldsymbol{\theta}_{\text{opt}}^{(0)} = [6, 6, \ldots, 6]$ which is the lower bound of the design region (denoted as Case A).
- $\boldsymbol{\theta}_{\text{opt}}^{(0)} = [8, 8, \ldots, 8]$ which is the midpoint of the design region (denoted as Case B);
- $\boldsymbol{\theta}_{\text{opt}}^{(0)} = [10, 10, \ldots, 10]$ which is the upper bound of the design region (denoted as Case C).

Fig. 10 shows the evolution of the objective function and FPF estimates (as well as the corresponding C.o.V.'s) with respect to the number of iterations for a given number of iterations $K = 19$. It is can be seen from the figure that, no matter which initial design is considered, the proposed combination algorithm with weight function $w_k^c(\boldsymbol{\theta})$ shows advantages, as it can obtain more accurate FPF estimate (with lower C.o.V.'s) and thus results in further gains on robustness and efficiency over ALS.

4.4. Example 4: Thermal Stress Analysis of Jet Engine Turbine Blade

The fourth example considers a jet engine turbine blade, as shown in Fig. 11. This blade has interior cooling ducts, through which the flow of cool air maintains the temperature of the blade within the limit for its material. The turbine is a radial array of blades typically made of nickel alloys. These alloys resist the extremely high temperatures of the gases. At such temperatures, the material expands significantly, producing mechanical stress in the joints and significant deformations of several millimetres. To avoid mechanical failure and friction between the tip of the

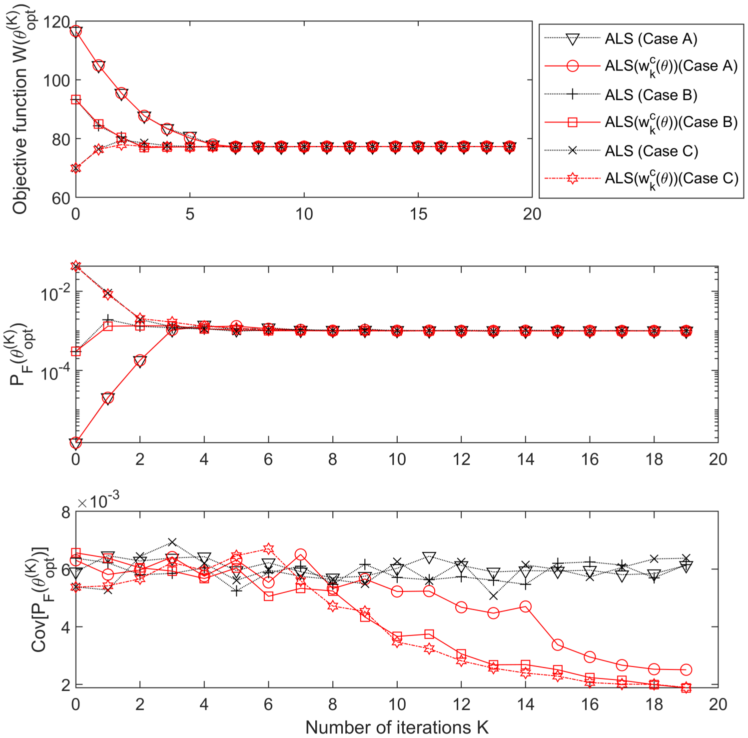

Figure 10: Evolution of the objective function and failure probability by the proposed approach (Example 3).

blade and the turbine casing, the blade design must account for the mechanical stresses and deformations. Failure is as such in this case defined as the maximum von Mises stress of the structure exceeding the given allowable value $\sigma_a = 1.5$GPa, and the corresponding limit state function is:

$$g(\boldsymbol{x}) = \sigma_a - \sigma_{max}(\boldsymbol{x}) \tag{50}$$

where $\sigma_{max}(\boldsymbol{x})$ is the maximum von Mises stress of the blade caused be the combination of thermal and pressure effects; $\boldsymbol{x} = [T_2, \gamma_{CTE}, \upsilon, P_1, P_2, K_{app}, T_1]$ is the vector of basic random variables; E, υ, γ_{CTE} and K_{app} are the Young's modulus, Poisson's ratio, coefficient of thermal expansion and the thermal conductivity for nickel-based alloy (NIMONIC 90), respectively; P_1 and P_2 are the pressure loads on the pressure and suction sides of the blade which is due to the high-pressure gas surrounding these sides of the blade; T_1 is the temperature of the interior cooling air and T_2 is temperature on the pressure and suction sides. All these variables are assumed to be independent truncated normal random variables and their distribution parameters are given in Table 7.

There are two design parameters which are of interest in this example, $\boldsymbol{\theta} = [\mu_{T_2}, \mu_{\gamma_{CTE}}]$, which are the mean values of γ_{CTE} and T_2, and they change over the domains $\theta_1 \in [800, 1200]$(°C) and

$\theta_2 \in [12, 16]$ (1/K), respectively. The corresponding RBDO problem is

$$\begin{aligned} \min_{\boldsymbol{\theta}} \quad & W(\boldsymbol{\theta}) = -\theta_1\theta_2, \\ \text{s.t.} \quad & P_F(\boldsymbol{\theta}) \leq 10^{-3}, \\ & 800 \leq \theta_1 \leq 1000, \quad 12 \leq \theta_2 \leq 16, \end{aligned} \tag{51}$$

where $W(\boldsymbol{\theta}) = -\theta_1\theta_2$ is the objective function related to the performance of the jet engine and the cost of the material.

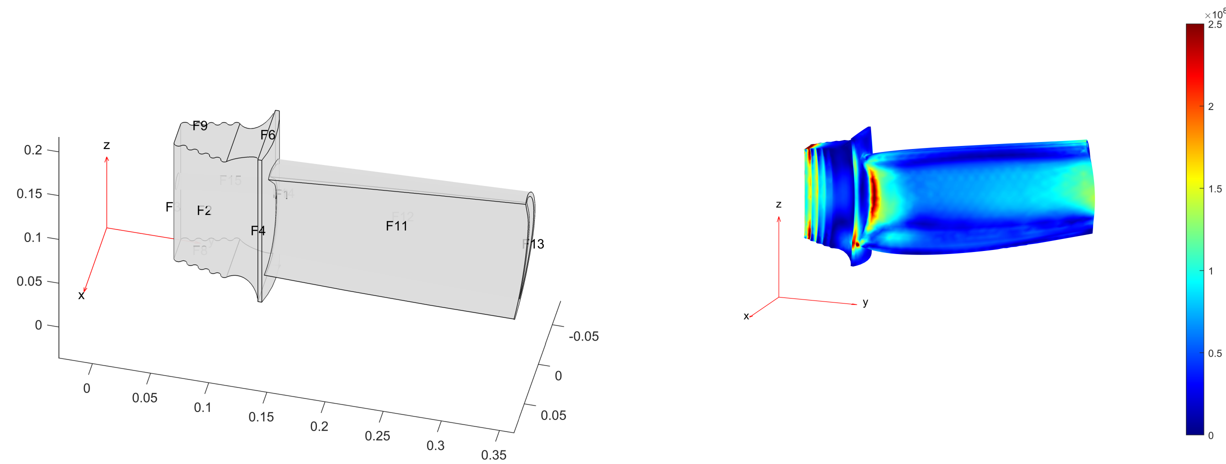

Figure 11: The geometry and von Mises stress of a turbine blade (Example 4).

Table 7: The distribution information of the basic random variables (Example 4).

Random variable	Mean value	Standard deviation
T_2(°C)	$\theta_1 = \mu_{T_2} \in [800, 1200]$	100
$\gamma_{\text{CTE}}(10^{-6})(1/\text{K})$	$\theta_2 = \mu_{\gamma_{\text{CTE}}} \in [12, 16]$	1.4
E(GPa)	250	23
υ	0.27	0.027
P_1(kPa)	500	50
P_2(kPa)	450	45
K_{app}(W/m/K)	11.5	1.15
T_1(°C)	150	15

Table 8: Results of optimization by different approaches (Example 4)

	$W(\boldsymbol{\theta}_{\text{opt}}^{(K)})(\times 10^5)$	$P_F(\boldsymbol{\theta}_{\text{opt}}^{(K)})$(C.o.V.)	$\boldsymbol{\theta}_{\text{opt}}^{(K)}$	$K \times N^{(K)}$
ALS($w_k^c(\boldsymbol{\theta})$) (Case A)	-1.3998	$1.0 \times 10^{-3}(0.005)$	$[1166.5, 12.0]$	5×400
ALS($w_k^c(\boldsymbol{\theta})$) (Case B)	-1.3999	$9.9 \times 10^{-4}(0.005)$	$[1166.6, 12.0]$	3×400
ALS($w_k^c(\boldsymbol{\theta})$) (Case C)	-1.4006	$1.0 \times 10^{-4}(0.004)$	$[1167.1, 12.0]$	5×400
Decoupling LP	-1.4005	$9.9 \times 10^{-3}(0.008)$	$[1167.1, 12.0]$	$4 \times (3 \times 400)$
Decoupling QP	-1.4010	$9.9 \times 10^{-3}(0.008)$	$[1167.5, 12.0]$	$4 \times (5 \times 400)$
Brute-force approach#	-1.3920	–	$[1160, 12]$	–

#The result of this brute-force approach is shown in Fig. 12.

The proposed approach with weights minimizing C.o.V. is applied to solve this challenging problem involving a finite element model. A number of $N = 400$ samples are used for ALS in each decoupling step. Different initial design settings are set to carry out the optimization i.e.,

- $\boldsymbol{\theta}_{\text{opt}}^{(0)} = [800, 12]$ which is the lower bound of the design region (denoted as Case A).
- $\boldsymbol{\theta}_{\text{opt}}^{(0)} = [1000, 14]$ which is the midpoint of the design region (denoted as Case B);
- $\boldsymbol{\theta}_{\text{opt}}^{(0)} = [1200, 16]$ which is the upper bound of the design region (denoted as Case C).

Table 8 lists the obtained results by different approaches. It can be seen from the table that the results of different approaches are approximately consistent. Among these approaches, the proposed approach is the most efficient. Note that the Double loop approach is not adopted in this example due to the computational burden. Instead, another brute-force approach is applied to approximate the global solution which is illustrated in Fig. 12.

In Fig. 12, a number of grid points are uniformly selected to fill the design region, 10 points for each dimension, thus a total of 100 points are considered. And the failure probability corresponding to each grid point is calculated by utilizing LS with 400 samples. Then, the points satisfying the constraints are represented by a 'circle', which are located in the feasible region; otherwise, the grid points are marked with a 'cross', indicating that they are located in the infeasible region. Form the figure, it is straightforward to determine the approximate optimal solution $\boldsymbol{\theta}_{\text{opt}} = [1160, 12]$, which is quite close to the obtained solutions listed in Table. 8. Fig. 12 also shows the trajectories of the optimization solutions of different cases, i.e., Cases A, B and C. It can be seen that the proposed approach converges very fast as it only requires 2-3 steps to reach the optimal solution.

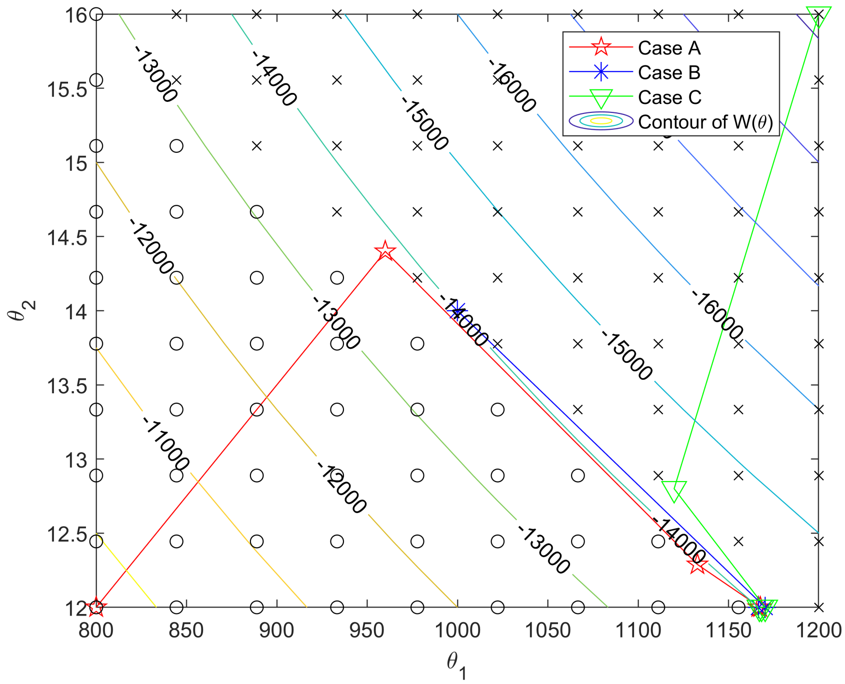

Figure 12: The trajectories of the solutions of different cases (A, B and C) by the proposed approach (Example 4). (Crosses denote infeasible designs and circles denote feasible designs.)

4.5. Final remarks

The results of the above examples have demonstrated the effectiveness of the proposed decoupling approach for solving RBDO problems. The success of the approach lies in that the FPF for decoupling is estimated by a single run of Line Sampling and the combination algorithm. For problems with a considerable number of design parameters (for example, 10 parameters in the third example), the optimal combination based on C.o.V. can further improve the efficiency of the proposed approach.

In the proposed combination algorithm, several weight functions are introduced. Here, $w_k^c(\boldsymbol{\theta})$ can improve the performance of the proposed approach for most cases (as shown in Examples 1 and 3). The alternative weights $w_k^a(\boldsymbol{\theta})$ and $w_k^v(\boldsymbol{\theta})$ sometimes can outperform the proposed approach. However, these weight functions cause the algorithm to be not as stable as when $w_k^c(\boldsymbol{\theta})$ is applied since their performance is problem-dependent.

5. Conclusions

This contribution presents a decoupling approach for structural RBDO problems based on Augmented Line Sampling (ALS) and a combination algorithm. It adopts ALS to efficiently obtain the FPF estimate, which is utilized to decouple the original RBDO problem. Further, the FPF estimate is used in conjunction with the concept of sequential optimization to iteratively update the FPF as the RBDO optimization progresses. To further optimize the efficiency, a combination algorithm is presented to re-use the FPF's which were evaluated in previous iterations of the sequential optimization.

Numerical as well as engineering examples are adopted to demonstrate the performance of the proposed approach. It can be concluded that the proposed approaches can obtain the optimal RBDO solution more efficiently than the tested decoupling approach based on Linear and Quadratic approximations, and the double loop approach. Further, the proposed approach based on ALS and the combination algorithm is more robust than the approach that just uses ALS.

The overall performance of the proposed approach is quite related to the ability of Line sampling to solve the associated reliability problem. This implies that addressing problems with highly nonlinear limit state functions may be a challenging task. Therefore, future research efforts will aim at expanding its range of application. Issues such as high dimensional reliability problems and nonlinearities/non-Gaussianity will be further explored. In addition, with the weighted approach developed herein, it is possible to construct approximations in small domains which can then be easily expanded towards larger domains.

Acknowledgements

Xiukai Yuan would like to acknowledge financial support from the Aeronautical Science Foundation of China (Grant No. ASFC-20170968002). Baoqiang Zhang acknowledges the financial support from National Science and Technology Major Project (Grant No. 2019-I-0006-0006), Special Project on the Integration of Industry, Education and Research of AECC (Grant No. HFZL2020CXY004 and HFZL2020CXY009).

Declarations

Conflict of interest

On behalf of all authors, the corresponding author states that there is no conflict of interest.

References

[1] M. A. Valdebenito, G. I. Schuëller, A survey on approaches for reliability-based optimization, Structural and Multidisciplinary Optimization 42 (2010) 645–663.

[2] D. Jerez, H. Jensen, M. Beer, Reliability-based design optimization of structural systems under stochastic excitation: An overview, Mechanical Systems and Signal Processing 166 (2022) 108397.

[3] I. Enevoldsen, J. D. Sørensen, Reliability-based optimization in structural engineering, Structural safety 15 (1994) 169–196.

[4] J. Liang, Z. P. Mourelatos, J. Tu, A single-loop method for reliability-based design optimisation, International Journal of Product Development 5 (2008) 76–92.

[5] T. Zou, S. Mahadevan, A direct decoupling approach for efficient reliability-based design optimization, Structural and Multidisciplinary Optimization 31 (2006) 190.

[6] M. Gasser, G. I. Schuëller, Reliability-based optimization of structural systems, Mathematical Methods of Operations Research 46 (1997) 287–307.

[7] H. A. Jensen, Structural optimization of linear dynamical systems under stochastic excitation: a moving reliability database approach, Computer methods in applied mechanics and engineering 194 (2005) 1757–1778.

[8] J. Ching, Y.-H. Hsieh, Local estimation of failure probability function and its confidence interval with maximum entropy principle, Probabilistic Engineering Mechanics 22 (2007) 39–49.

[9] J. Ching, Y.-H. Hsieh, Approximate reliability-based optimization using a three-step approach based on subset simulation, Journal of engineering mechanics 133 (2007) 481–493.

[10] X. Yuan, Local estimation of failure probability function by weighted approach, Probabilistic Engineering Mechanics 34 (2013) 1–11.

[11] X. Yuan, Z. Lu, Efficient approach for reliability-based optimization based on weighted importance sampling approach, Reliability Engineering & System Safety 132 (2014) 107–114.

[12] M. G. Faes, M. A. Valdebenito, Fully decoupled reliability-based design optimization of structural systems subject to uncertain loads, Computer Methods in Applied Mechanics and Engineering 371 (2020) 113313.

[13] P. Ting Lin, H. Chang Gea, Y. Jaluria, A modified reliability index approach for reliability-based design optimization, Journal of Mechanical Design 133 (2011).

[14] J. Tu, K. K. Choi, Y. H. Park, A new study on reliability-based design optimization, Journal of Mechanical Design 121 (1999) 557–564.

[15] B. D. Youn, K. K. Choi, L. Du, Enriched performance measure approach for reliability-based design optimization., AIAA journal 43 (2005) 874–884.

[16] S.-K. Au, J. L. Beck, A new adaptive importance sampling scheme for reliability calculations, Structural safety 21 (1999) 135–158.

[17] X. Yuan, Z. Lu, C. Zhou, Z. Yue, A novel adaptive importance sampling algorithm based on markov chain and low-discrepancy sequence, Aerospace Science and Technology 29 (2013) 253–261.

[18] M. A. Misraji, M. A. Valdebenito, H. A. Jensen, C. F. Mayorga, Application of directional importance sampling for estimation of first excursion probabilities of linear structural systems subject to stochastic Gaussian loading, Mechanical Systems and Signal Processing 139 (2020) 106621.

[19] S.-K. Au, J. L. Beck, Estimation of small failure probabilities in high dimensions by subset simulation, Probabilistic engineering mechanics 16 (2001) 263–277.

[20] H. Pradlwarter, G. I. Schuëller, P.-S. Koutsourelakis, D. C. Charmpis, Application of line sampling simulation method to reliability benchmark problems, Structural Safety 29 (2007) 208–221.

[21] M. A. Valdebenito, P. Wei, J. Song, M. Beer, M. Broggi, Failure probability estimation of a class of series systems by multidomain line sampling, Reliability Engineering & System Safety 213 (2021) 107673.

[22] B. D. Youn, K. K. Choi, A new response surface methodology for reliability-based design optimization, Computers & Structures 82 (2004) 241–256.

[23] C. Kim, K. K. Choi, Reliability-based design optimization using response surface method with prediction interval estimation, Journal of Mechanical Design 130 (2008).

[24] H. Zhang, Y. Aoues, D. Lemosse, E. S. de Cursi, A single-loop approach with adaptive sampling and surrogate kriging for reliability-based design optimization, Engineering Optimization (2020) 1–17.

[25] H. Jensen, D. Jerez, M. Valdebenito, An adaptive scheme for reliability-based global design optimization: A markov chain monte carlo approach, Mechanical Systems and Signal Processing 143 (2020) 106836.

[26] X. Yuan, Z. Zhenxuan, Z. Baoqiang, Augmented line sampling for approximation of failure probability function in reliability-based analysis, Applied Mathematical Modelling 80 (2020) 895–910.

[27] J. Song, M. Valdebenito, P. Wei, M. Beer, Z. Lu, Non-intrusive imprecise stochastic simulation by line sampling, Structural Safety 84 (2020) 101936.

[28] J. Jacobs, L. Etman, F. Van Keulen, J. Rooda, Framework for sequential approximate optimization, Structural and Multidisciplinary Optimization 27 (2004) 384–400.

[29] I. Papaioannou, D. Straub, Combination line sampling for structural reliability analysis, Structural Safety 88 (2021) 102025.

[30] X. Yuan, Y. Qian, J. Chen, M. Faes, M. Valdebenito, M. Beer, Global failure probability function estimation based on an adaptive strategy and combination algorithm, Reliability Engineering & System Safety 231 (2023) 108937.

[31] X. Yuan, Y. Qian, J. Chen, M. G. Faes, M. A. Valdebenito, M. Beer, Global failure probability function estimation based on combination and adaptive strategy, preprint submitted to Elsevier (2022).

[32] S. Song, Z. Lu, H. Qiao, Subset simulation for structural reliability sensitivity analysis, Reliability Engineering & System Safety 94 (2009) 658–665.

[33] S. Xiao, Z. Lu, Structural reliability analysis using combined space partition technique and unscented transformation, Journal of Structural Engineering 142 (2016) 04016089.